

Stability analysis of the commensurate monolayer solid of xenon/graphite

L. W. Bruch¹ and A. D. Novaco²¹*Department of Physics, University of Wisconsin-Madison, Madison, Wisconsin 53706, USA*²*Department of Physics, Lafayette College, Easton, Pennsylvania 18042, USA*

(Received 8 January 2008; revised manuscript received 4 March 2008; published 27 March 2008)

A stability analysis based on model calculations of the grand potential finds that the transition from hexagonal incommensurate to commensurate monolayer solid of xenon/graphite is continuous with increasing pressure, in agreement with experimental observations. An atomic-scale interaction model gives an internally consistent account of the thermal expansion of the solid at the two-dimensional sublimation curve and of the chemical potential increase for isothermal compression from monolayer condensation to the commensurate solid. An estimate is given for the corrugation energy of xenon/graphite.

DOI: [10.1103/PhysRevB.77.125435](https://doi.org/10.1103/PhysRevB.77.125435)

PACS number(s): 68.43.-h, 64.70.Rh, 63.22.-m, 68.65.-k

I. INTRODUCTION

Although many features of the phase diagram of monolayer xenon adsorbed on the basal plane surface of graphite are well-established experimentally and understood in terms of the atomic interactions,¹⁻³ there remain some troubling contradictions between experiment and theory. One of the most conspicuous is for the order of the commensurate-incommensurate transition. Experimentally, the transition to a commensurate monolayer solid (C) under increasing pressure is found to be continuous from a hexagonal incommensurate (HI) solid to the $(\sqrt{3} \times \sqrt{3})R30^\circ$ structure.^{4,5} The conclusion of rather general theoretical arguments^{6,7} is that a HI→C transition should be first order (discontinuous) and that a continuous transition should be via a uniaxially incommensurate (UIC) lattice. In the experiments,^{4,5} any discontinuity in lattice constant at about 60 K must be smaller than 0.2%.

In this paper, we extend the stability analysis of Bak *et al.*⁶ to cover a transition under pressure using the grand potential. We note that the qualitative density dependencies of the free energy anticipated by Bak *et al.* were not present in the model calculations of Joos *et al.*,⁸ which do support the occurrence of a continuous HI→C transition for Xe/graphite. Finally, we use the stability analysis to make an estimate of the energy corrugation of the minimum potential energy surface of xenon interacting with basal plane graphite from fits to the chemical potential increase $\Delta\mu$ at $T=60$ K from monolayer condensation to the onset of the $(\sqrt{3} \times \sqrt{3})R30^\circ$ monolayer solid.

The organization of this paper is as follows. Section II contains a description of the components of the calculation. Section III presents the stability analysis and Sec. IV the application to Xe/graphite. Concluding remarks are given in Sec. V. There is an appendix on the zeroth-order form of the self-consistent-phonon, mass-density-wave (SCP-MDW) approximation for monolayers. The basic ideas of the general formulation of this approximation are contained in two earlier papers.^{9,10} The Appendix outlines how this approximation is derived; it amounts to a simple modification of previously published work, namely, the linear response version of the SCP-MDW approximation.⁹

II. COMPONENTS OF THE CALCULATION

A. Interactions and structures

This is a two-dimensional (2D) calculation in which the xenon positions are constrained to lie in a plane. The Xe-Xe interactions are the HFD-B2 pair potential¹¹ augmented by the McLachlan substrate mediated dispersion energy¹² with parameters $C_{s1}=142$ a.u., $C_{s2}=89$ a.u., and $L_{ov}=1.9$ Å. The overlayer height L_{ov} is constructed from a measured height of 3.6 Å of commensurate xenon above the surface layer of carbon atoms¹³ and the spacing between the graphite basal planes. No adsorption-induced static dipole moment terms are included because the work function change^{14,15} is only 10%–20% of that for xenon on metals and the effect of the dipole term for Xe/Ag(111) is quite small.¹⁶

The corrugation potential energy is parametrized using only the first shell of reciprocal lattice vectors \mathbf{g} of graphite:²

$$V_s(\mathbf{r}) = V_g \sum_{\mathbf{g}} \exp(i\mathbf{g} \cdot \mathbf{r}), \quad (1)$$

where the origin of \mathbf{r} is at the center of a carbon hexagon and values of V_g in the range -3.7 to -10 K are used. This range is similar to that used by Joos *et al.*, with small magnitudes leading to incommensurate lattices of minimum potential energy and large magnitudes having the $(\sqrt{3} \times \sqrt{3})R30^\circ$ lattice as minimum potential energy state. The main source of information on V_g has been calculations¹⁷ of the adsorption energy of Xe/graphite using pair potential models and the values range from $V_g=-4$ to -12 K. A value $V_g=-4.4$ K was estimated¹⁸ by a fit to the intensity of modulation satellites in x-ray diffraction from the incommensurate monolayer solid, while the value obtained in a recent electronic energy calculation¹⁵ is $V_g \approx -8$ K.

Two sets of structures are treated. For that set used in the quasiharmonic lattice dynamics (QHT) calculations, a series of higher-order-commensurate (HOC) lattices is constructed with a rule similar to one adopted^{19,20} for structures of Xe/Pt(111). The unit cell has N^2 atoms and primitive vectors

$$\mathbf{A}_1 = (N+1)\mathbf{a}_1 + N\mathbf{a}_2, \quad \mathbf{A}_2 = -N\mathbf{a}_1 + (2N+1)\mathbf{a}_2, \quad (2)$$

where \mathbf{a}_1 and \mathbf{a}_2 are primitive vectors (length $\ell=2.46$ Å) of the basal plane graphite surface and the initial positions of the xenons, before relaxation of forces, are in a hexagonal

(triangular) lattice with primitive vectors \mathbf{A}_1/N and \mathbf{A}_2/N . The nearest-neighbor spacing in the average lattice is $\bar{L} = L_c[1 + (1/N) + (1/3N^2)]^{1/2}$, with $L_c = \ell\sqrt{3} \approx 4.26 \text{ \AA}$, and the misfit m is defined by $\bar{L} = L_c(1+m)$. As the choice of N increases from 8 to 30, the average spacing and misfit decrease from $\bar{L} = 4.53 \text{ \AA}$, $m = 0.0631$ to $L = 4.33 \text{ \AA}$, $m = 0.0167$. This covers most of the range of observed monolayer solids of Xe/graphite,^{1,4} although the misfits $m < 0.01$ are treated by extrapolation. These lattices are rotated from the 30° orientation by angles $\vartheta = 1.9^\circ - 0.5^\circ$. This construction is an efficient way to generate HOC unit cells with average densities in the observed range of Xe/graphite, and the alignments at modest to large misfits agree well with the results of the zeroth-order SCP-MDW approximation (Appendix).^{9,10} However the experimental data^{4,18,21} for the orientational epitaxy differ from these model results by generally having smaller ϑ and a transition to $\vartheta = 0$ at large misfit near 100 K. Nevertheless, the energy shifts that arise from these orientation differences are small, and we believe that the model structures are sufficiently realistic to recover the major features of the monolayer equation of state of Xe/graphite.

A different set of initially aligned lattices with small misfits is generated for the molecular dynamics (MD) calculations. These linear misfits are in the range $m = 0.001$ to $m = 0.03$. Two classes of systems are examined, both using periodic boundary conditions on rectangular boxes that include an integer number of graphite unit cells. In the constrained class, the xenon lattice fills the entire box and is effectively under external pressure. In the unconstrained class, a xenon patch covers from about 50% to about 90% of the box. Since the unconstrained simulations are done at a relatively low temperature, there are very few xenon atoms in the 2D-gas phase and so these patches are at nearly zero pressure. The time step for all simulations is 32.6 fs (1% of the characteristic time $R_{\min}\sqrt{m_{\text{Xe}}}/\epsilon$ for xenon moving in the HFD-B2 potential). The thermal averages were done in blocks of 1000 time steps and stored for later analysis and further averaging. The autocorrelation time for the data reported here is generally less than the time interval associated with one block, so that the block averages can be treated as statistically independent. The cutoff radius for the force is such that there are, on the average, 36 neighbors of the central particle within this radius. While the forces due to particles beyond this range are ignored, the corresponding potential energy contributions are included by using a uniform density model and integrating the potential energy out to infinity. With these parameters, energy conservation is maintained to at least five significant figures over a minimum of 200 000 time steps at the highest temperatures considered here.

In all the simulations, the initial xenon configuration is a centered rectangular lattice that is constrained to be a superlattice of the graphite basal plane surface lattice. For the unconstrained class, the aspect ratio of the simulation cell is nearly 1:1, and there are approximately 20 K (20064) xenon particles initially arranged in a configuration of 152 rows by 132 columns. On the other hand, the aspect ratio of the simulation rectangle for the constrained class is approximately $1:\sqrt{3}/2$, except for those simulations in which the system is forced into the UIC structure (see Sec. IV C 3). The initial

configurations for the constrained class have n rows by n columns of xenon atoms with $n=64$, $n=128$, or $n=256$. We refer to these sizes as 4 K (4096), 16 K (16 384), and 64 K (65 536), respectively. Most of the simulation data reported here are for the 16 K size, and no serious size dependence was observed in these data as judged by comparisons of low-order polynomial fits to the isochores. The fit parameters for the 16 K and 64 K systems (for the same density) are almost the same within statistical uncertainty, and the ground state and low temperature values of the energy for these systems are the same to nearly five significant figures.

B. Energy and free energy

The first step is to find the minimum potential energy structure for a given HOC cell. For both sets of structures, this is obtained using a modified MD calculation, in the QHT series by successively relaxing the positions to reduce the force on a configuration and in the MD series by reducing an effective temperature to let the dynamics seek out the lowest energy configuration.

Then, the Helmholtz free energies are constructed in the QHT approximation^{2,22} for the structures obtained using Eq. (2). The frequencies come from the eigenvalues of real symmetric matrices of order $4N^2$, i.e., for $N=8-30$ the order increases from 256 to 3600. A basic stability and convergence check on the force relaxation is that all the eigenvalues must be positive. The summation over the Brillouin zone is evaluated by a special point sampling.²³ The Helmholtz free energy is used to determine the monolayer equation of state. It yields the zero temperature structure, the thermal expansion of the average lattice constant L_u of the unconstrained (minimum free energy) solid, and the chemical potential of the compressed solid. The QHT approximation is known to overestimate the thermal expansion as the melting temperature is approached, but tests in the present work show that the $L_u(T)$ remains accurate up to 60 K. Various aspects of the QHT calculations are checked against two very different types of calculations, namely, a set of self-consistent-phonon calculations (SCP for the C-lattice and SCP-MDW for the HI lattices) at $T=0-60$ K and a set of MD calculations near $T=60$ K.

The MD calculations are standard two-dimensional NVE ensemble simulations,²⁴ using periodic boundary conditions, for the xenon layer in the presence of the graphite substrate. The temperature is obtained from the kinetic energy using the equipartition theorem. The MD calculations for the constrained cells provide, in the limit of zero temperature, a check on the potential energy obtained for the HOC cells in the initial stage of the QHT calculations. Static potential energies from the two calculations for a given density agree to 0.5–1 K out of approximately 800 K per xenon, Table I. Finite temperature MD results compare well to the average energies of both SCP and QHT calculations as discussed below. The MD calculations for the unconstrained cells are used to check the structures and zero pressure lattice constants L_u obtained in the higher temperature range of the QHT calculations.

The zeroth-order SCP-MDW approximation treats the distortions of the xenon layer resulting from $V_s(\mathbf{r})$ in an ap-

TABLE I. Xenon/graphite QHT and MD static potential energies Φ_0 and MD and SCP-MDW increments $\Delta\Phi$ in average potential energy at the specified average kinetic energies $\langle\text{KE}\rangle$ and lattice constants \bar{L} . The QHT and MD incommensurate lattices have slightly different orientations ϑ ; unless otherwise noted $\vartheta=0$. MD values are classical mechanical time averages with temperature equal to $\langle\text{KE}\rangle/k_B$. The SCP-MDW and QHT energies $\langle\text{KE}\rangle$ and $\Delta\Phi$ include quantum corrections, and the temperatures near 60 K are 2–3 K less than $\langle\text{KE}\rangle/k_B$. Lengths are in Å and energies (per atom) are in Kelvin.

\bar{L}^a	V_g	Φ_0 (QHT)	Φ_0 (MD)	$\langle\text{KE}\rangle$	$\Delta\Phi$ (MD)	$\Delta\Phi$ (SCP) ^{b,c}
4.2608	0.0	-755.1	-755.1	63.2	62.7	60.1
	-5.0	-785.1	-785.1		62.8	60.4
	-8.0	-803.1	-803.1		62.8	60.6
4.3385	0.0	-780.3 ^d	-780.3	62.4	61.3	58.2
	-5.0	-788.1 ^d	-788.0		61.3	60.1
	-8.0	-797.6 ^d	-797.6		61.5	60.7
4.4606	0.0	-772.5 ^e	-772.5	61.6	59.1	54.8
	-5.0	-774.8 ^e	-774.6		59.0	56.2
	-8.0	-778.5 ^{e,f}	-778.1		58.8	58.0

^aNearest-neighbor spacing in the corresponding average triangular lattice.

^bIncrement in average potential energy relative to the static lattice evaluated using the zeroth-order MDW approximation.

^cFor the QHT approximation, $\Delta\Phi(\text{QHT})=\langle\text{KE}\rangle$.

^d $\vartheta=0.58^\circ$.

^e $\vartheta=1.44^\circ$.

^fThe Novaco-McTague perturbation theory gives a difference of 0.5 K in the mass-density-wave energy between $\vartheta=1.44^\circ$ and $\vartheta=0^\circ$ at this \bar{L} and V_g .

proximate but realistic fashion. These SCP-MDW calculations provide tests of the QHT free energy calculations in the large ($m > 0.02$) misfit region, as well as providing estimates of temperature-dependent shifts in the phonon spectrum and of substrate-driven modulation energies of the incommensurate monolayer for small distortions. The zero pressure SCP-MDW values L_u agree with the QHT values to 0.01 Å up to 40 K and to 0.02 Å at 60 K, where the QHT values are greater than the SCP-MDW values. We consider this to be good agreement and consistent with previous experience with application of the QHT approximation to monolayer thermal expansion.²

A direct comparison of the SCP and QHT results for the C lattice shows the Helmholtz free energies agree to a couple tenths of a Kelvin at low temperatures and to a couple of Kelvin at the highest temperatures used here ($T \approx 60$ K). For the HI structures, the zeroth-order SCP-MDW results for L_u and the free energy merge with the QHT results at low temperatures and moderate to large misfit values. Both the QHT and SCP-MDW values for $L_u(T)$ merge with the MD results for unconstrained layers at temperatures of 50–60 K. The QHT and SCP-MDW results for the dynamical Helmholtz free energy term differ by about 10 K out of 90 K per xenon at $T=60$ K, which is consistent with previous comparisons of approximations for Xe/Ag(111).²⁵ The MD, QHT, and SCP-MDW methods give very similar values for the average potential energy at the same average kinetic energy in the near-classical limit ($T \approx 60$ K). This is evident in the results for three average lattice constants and three values of the corrugation amplitude V_g presented in Table I. The increase

$\Delta\Phi$ (MD) in the MD average potential energy relative to its static lattice value is nearly equal to the temperature. This is the result expected for a harmonic lattice and shows that the lattice remains nearly harmonic at 60 K. Also, as expected, the anharmonic effects are larger for more dilated lattices. The QHT and SCP-MDW values bracket $\Delta\Phi$ (MD), with the SCP-MDW approximation most likely overestimating the amount of anharmonic shift. The values $\Delta\Phi$ (SCP-MDW) have more dependence on V_g than the QHT values at $T=60$ K, where a variation of 0.2 K with V_g is found at constant L ; this appears to be a consequence of the temperature-dependent shifts in the SCP phonon spectrum. However, these differences do not affect the conclusions of this paper. In summary, there appear to be no major unresolved discrepancies between the various approaches.

III. STABILITY ANALYSIS

The stability comparisons are for adsorption on an area A at temperature T as a function of chemical potential μ . The 2D density n is expressed as the ratio to the commensurate density n_c , $\theta=n/n_c$. We assume the Helmholtz free energy per atom f at temperature T can be approximated for $\theta \approx 1$ by

$$f \approx f_c + (\theta - 1)f_1 + \frac{1}{2}(\theta - 1)^2 f_2. \quad (3)$$

(In terms of the domain wall energy per length w_1 at very small misfit and the commensurate length L_c , the first coefficient is $f_1 = -3L_c w_1/2$). In the following discussion, we

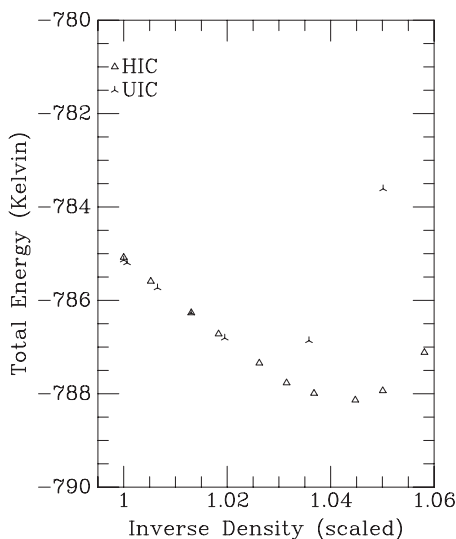


FIG. 1. Potential energy per particle versus scaled area (inverse number density $1/\theta$) for both HI and UIC structures, with the HFD-B2 pair potential augmented by the McLachlan interaction and $V_g = -5$ K. Energies are those for the zero temperature limit of finite temperature MD runs on constrained cells of size 128×128 (HI) and 10×1024 (UIC). Note that the HI and UIC energies merge to within the accuracy of the calculation at $1/\theta < 1.015$. Uncertainties in the energies are much smaller than the plotted symbols.

have in mind the situation for monolayer Xe/graphite where the adatoms condense in an incommensurate lattice of lower density than the commensurate one, i.e., $\theta < 1$, and at sufficiently low temperature ($T < 65$ K) can be compressed into a commensurate lattice before the bilayer solid forms. For Eq. (3), this becomes a condition $f_1 > 0$, i.e., $w_1 < 0$ and domain walls form spontaneously.

The potential energy calculations of Joos *et al.*⁸ (which are consistent with our work, Fig. 1) show that uniaxially incommensurate (UIC) and hexagonal incommensurate (HI) lattices of the same density, near the commensurate (C) value ($\theta = 1 - \xi$ and $\xi \downarrow 0$), have the same values of f_1 and that the curvature is larger for the UIC lattice, $f_2(\text{UIC}) > f_2(\text{HI})$. In the language of Bak *et al.*,⁶ the properties $f_1 > 0$ and $f_2(\text{UIC}) > f_2(\text{HI})$ would be attributed to attractive domain wall crossings in the HI lattice. However, the following analysis shows that, for a model with these properties, the HI lattice is stable relative to the UIC lattice for θ near 1 and that the HI \rightarrow C transition is continuous as a function of increasing pressure (or μ).

The grand potential for N atoms at chemical potential μ and temperature T is expressed in terms of the total Helmholtz free energy $F_N = Nf$ by

$$\Omega = F_N - N\mu = N(f - \mu) = N_c \theta (f - \mu). \quad (4)$$

At specified total area and temperature, the equilibrium state has minimum Ω . If (as we assume)²⁶ the dependence of f on θ is smooth enough that the first two derivatives exist, the stationary condition is

$$\frac{\partial \Omega}{\partial \theta} = 0 \Rightarrow \mu = f + \theta \frac{\partial f}{\partial \theta}, \quad (5)$$

and the minimum condition is

$$\frac{\partial^2 \Omega}{\partial \theta^2} > 0 \Rightarrow 2 \frac{\partial f}{\partial \theta} + \theta \frac{\partial^2 f}{\partial \theta^2} > 0. \quad (6)$$

Close to the commensurate density, $\theta \approx 1$, Eq. (6) becomes $2f_1 + f_2 > 0$. This stability requirement is satisfied in the results of Joos *et al.*⁸ for condensation into states of $\theta < 1$.

Now, examine the results of the stability analysis for Eq. (3) at densities near the commensurate density. The stationary condition [Eq. (5)] becomes

$$\mu = f_c + f_1 - (2f_1 + f_2)\xi + \frac{3}{2}f_2\xi^2. \quad (7)$$

Define $\delta\mu = \mu - f_c - f_1$; then, $\delta\mu < 0$ as the C phase is approached by compression (increasing μ). Inverting Eq. (7) gives an estimate for ξ at specified $\delta\mu$ (Ref. 27):

$$\xi = -\frac{\delta\mu}{(2f_1 + f_2)} + \frac{3}{2} \frac{f_2(\delta\mu)^2}{(2f_1 + f_2)^3} + \dots \quad (8)$$

To decide the relative stability of the UIC and HI phases at specified chemical potential, we compare the grand potentials

$$\frac{\Omega}{N_c} \approx f_1 - \delta\mu - \frac{2(\delta\mu)^2}{(2f_1 + f_2)}. \quad (9)$$

The HI structure has the smaller f_2 and thus the lower Ω . Therefore, the HI structure is stable relative to the UIC phase as $\xi \downarrow 0$.

We cannot exclude the possibilities that the considerations of Bak *et al.* become dominant at exceedingly small ξ , i.e., much smaller misfits than are treated in the model calculations or found in the experiments, or that very different interaction models would show the features they described. We do note that the strong interatomic repulsions in the Xe/graphite models lead to rather broad domain walls, and therefore the discussion in terms of wall energies and wall crossing energies must allow for density dependence of those parameters.

IV. MODEL CALCULATIONS AND EXPERIMENT

A. Summary of experimental data

In Sec. III, we assert that the Xe/graphite transition from incommensurate to commensurate solid (HI \rightarrow C) is continuous, based on qualitative features of the density dependence of the potential energy and the free energy. Here, as another application of the stability analysis, we make a quantitative comparison of experimental data for Xe/graphite with the results of our calculations. There are three major points: (1) The monolayer condenses as an incommensurate solid at least down to temperatures $T \approx 20$ K.^{18,28,29} (2) The monolayer condenses as an incommensurate solid with lattice constant L_u very similar to that of Xe/Ag(111) for $T = 40-80$ K.^{29,30} (3) The increment in chemical potential as

TABLE II. Quasiharmonic theory (QHT) for the thermal expansion and compression of Xe/graphite [L_u is the average (HI) lattice constant for minimum free energy $f(L_u)$; $\mu(L_c)$ is the chemical potential for the commensurate lattice obtained by compression, Eq. (7), and $\Delta\mu \equiv \mu(L_c) - f(L_u)$] for several corrugation energy amplitudes V_g . See Sec. IV B for discussion. Lengths are in Å and energies in Kelvin.

V_g	T (K)	Φ^a	1^b	20	40	50	60 ^c
-3.7	L_u	4.36	4.39	4.40	4.44	4.45	4.47
	$f(L_u)$	-786	-752	-763	-806	-837	-872
	$\mu(L_c)$	-535	-317	-255	-130	-68	-6
	$\Delta\mu$	251	435	508	676	769	866
-5.0	L_u	4.35	4.38	4.40	4.43	4.45	4.47
	$f(L_u)$	-788	-753	-765	-807	-838	-873
	$\mu(L_c)$	-683	-465	-402	-273	-208	-145
	$\Delta\mu$	105	288	363	534	630	728
-8.0	L_u	4.26	4.35	4.38	4.42	4.44	4.47
	$f(L_u)$	-803	-760	-770	-811	-841	-876
	$\mu(L_c)$	-803	-735	-665	-524	-459	-393
	$\Delta\mu$	0	25	105	287	382	483
-10.0	L_u	4.26	4.26	4.26	4.40	4.44	4.47
	$f(L_u)$	-815	-771	-777	-816	-845	-880
	$\mu(L_c)$	-815	-771	-777	-660	-589	-520
	$\Delta\mu$	0	0	0	156	256	360

^aInterpolate in slope f_1 , Eq. (3), to onset of commensurate ground state at $V_g = -6.2$ K.

^bInterpolate in slope f_1 to onset of commensurate ground state at $V_g = -8.4$ K.

^cAt 60 K, interpolate to $\Delta\mu = 675$ K at $V_g = -5.6$ K.

the monolayer solid is compressed from condensation to the commensurate solid is³¹ $\Delta\mu \approx 675$ K at 60 K and ≈ 590 K at 50 K.

Diffraction experiments definitely show that the Xe/graphite solid at monolayer condensation is incommensurate at low temperatures. There is some uncertainty in the lattice constant: Hong *et al.*¹⁸ report $L_u = 4.32$ Å at 25 K. Ellis *et al.*²⁸ give $L_u = 4.42$ Å at 15 K, and Mowforth *et al.*²⁹ give $L_u = 4.43$ Å at 20 K. The low temperature value of L_u in the model calculations is strongly affected by the value of V_g , and it is unfortunate that there is such a spread in the experimental values of L_u . We believe that the experimental conditions are such that the larger values of L_u should be relied on more because extraneous sources of compression could lead to smaller values of L and, in fact, this was observed in some preparations of the monolayer.²⁸

The values of L_u at 40 and 60 K are reported to be^{21,29} 4.44 and 4.47 Å, respectively. These are within 0.01 Å of the values reported for Xe/Ag(111) by Unguris *et al.*³⁰ The Xe-Xe interaction model used here for Xe/graphite is very similar to the one used for Xe/Ag(111), so that the similarity of the two sets of data becomes understood if (as does happen in the calculations) the thermal excitation effects greatly diminish the consequences of the substrate corrugation V_g for $T \approx 50$ K.

Finally, we note that the chemical potential increment from monolayer condensation to bilayer condensation derived from the phase diagram of Suzanne *et al.*^{3,32} is 780 K for $T = 60 - 70$ K.

B. Quasiharmonic lattice dynamics free energies

The experimental value for $\Delta\mu$ at $T = 60$ K is based on the experiments of Hamichi *et al.*⁴ for the HI \rightarrow C transition near 60 K and an extrapolation of the Suzanne *et al.* data³³ for the monolayer condensation pressure from the lowest observation temperature of 75 K. The value at $T = 50$ K is based on further extrapolations. Thus, $T = 50 - 60$ K is probably as low a temperature as can be used for the thermodynamic construction. It also corresponds to a rather high temperature for using quasiharmonic free energy constructions. We believe that the various checks on energy and free energy using the MD and SCP-MDW approximations ensure the utility of the QHT for calculating $\Delta\mu$ at these temperatures and that our analysis supersedes that of Kariotis *et al.*³⁴

Results based on cubic spline interpolations to the quasiharmonic free energies for the C lattice and nine values of N in the range 8–30 are presented in Table II. For the potential energies listed there, the lateral interactions are summed explicitly up to a cutoff distance of 12–15 Å and larger distances are included using a uniform lattice approximation.

There are four main conclusions to be drawn from Table II. (1) The range $V_g \leq -10$ K is excluded³⁵ by the fact that Xe/graphite is incommensurate at monolayer condensation at 20 K. (2) The role of the corrugation in setting L_u becomes negligible above 40 K, which is the reason for the similarity of L_u for Xe/Ag(111) and Xe/graphite. (3) The change in $\Delta\mu$ from $T = 50$ to 60 K is about 100 K, in good agreement with the extrapolations in the experimental phase diagram

which give ≈ 85 K. (4) The window in μ for the presence of the commensurate phase diminishes as the temperature increases; combining an extrapolation of the calculated $\Delta\mu$ to $T > 60$ K with the experimental chemical potential increment from monolayer to bilayer at 70 K, the calculations are consistent with the window closing before 70 K.

By interpolation of the results for the initial slope f_1 [Eq. (3)] as a function of V_g , and allowing for uncertainties in the free energy and the spline calculation of f_1 , we estimate that the commensurate lattice is the minimum potential energy configuration for $V_g \leq -(6 \pm 0.5)$ K and is the lowest total energy configuration for $V_g \leq -(8 \pm 0.5)$ K. The optimal choice of V_g to fit the experimental data is in the range -5 to -8 K, and probably close to -6 K. This gives $\Delta\mu$ reasonably close to the empirical values.³¹

C. Molecular dynamics simulation of domains

1. Energies and structure factors

The MD simulations of the constrained system are used to check the zero temperature QHT results for the energy and chemical potential and to examine domain structures of the incommensurate monolayer. Most of the simulation results reported here are for the 16 K system at various densities and kinetic energies. The system is usually initialized at moderate temperatures (well below melting), cooled to almost zero temperature, heated above the original temperature, typically above 60–70 K, and then cooled. A polynomial fit to the 15 points lowest in temperature (15–20 for the UIC series in Sec. IV C 3) is used to find the zero temperature energy and its uncertainty. There was no observable hysteresis for the constrained cells.

The MD and QHT configurations usually have slightly different orientations ϑ . The difference in the static potential energies Φ_0 of MD and (interpolated) QHT configurations of the same density but different ϑ gives an estimate of the effect of small misorientations. Some examples are given in Table I; such comparisons show that energy terms due to misorientation of the monolayer are probably negligible, being about 1 K or less in the range $\vartheta = 0^\circ - 3^\circ$ that is relevant here. The SCP-MDW results have a similar variation of the energy with ϑ . Thus, for the range of ϑ treated here, the error due to misalignment of the xenon monolayer is small enough that it may be ignored for determining L_u and $\Delta\mu$.

The MD data also provide a check on the calculation of $\Delta\mu$ at zero temperature. Two simple numerical differentiation schemes were used to find the (classical) chemical potential at $T = 0$ K and these values are compared to the QHT results (HOC static potential energies) for the change $\Delta\mu$ between the value at L_u and the value at the commensurate lattice constant L_c . For $V_g = -5.0$ K, both schemes give $\Delta\mu \approx 91$ K, rather than the value of 105 K listed in Table II. The 14 K difference is probably a good estimate of the uncertainty in the results. In addition, the MD energies agree with the QHT result, Table II, that the commensurate lattice is the minimum potential energy state for $V_g = -8$ and -10 K.

The MD simulations for the unconstrained system are used to test the results of the QHT and SCP-MDW approximations at the higher temperatures, especially for the thermal

expansion of the average (unconstrained) lattice constant $L_u(T)$. Structure factor calculations for the three smallest nonequivalent reciprocal vectors of these lattices are used to determine values of L_u with an estimated uncertainty of ± 0.01 Å. The static structure factor $S(\mathbf{q})$ is calculated using 50 000–100 000 time steps (1.63–3.26 ns) for \mathbf{q} vectors that are on a finer grid than those that satisfy the periodic boundary conditions. Thus, the structure factors are those of a finite patch and not the periodic continuation of the basic system. The peak positions in $S(\mathbf{q})$ are determined by a graphical analysis of contour plots of $S(\mathbf{q})$ in the \mathbf{q} plane. The widths of these peaks are consistent with the size of the system, and the placement of the peaks reflects the basic hexagonal structure of the system, often showing a slight lattice rotation, typically $\vartheta < 1^\circ$. For the larger values of $|V_g|$, small satellite peaks are observed but the signals tend to be noisy and difficult to analyze. Analysis of the constrained system typically shows a hexagonal lattice that is aligned with the C lattice, having a lattice constant consistent with the HI structure of the parent lattice.

There is significant hysteresis in the simulations for $V_g = -8$ and -10 K cases of the unconstrained system. For these values of V_g , the initial structure at very low temperatures is the commensurate lattice, in agreement with the static potential energy calculations presented in Table II. As the system is heated, domain walls form and, at high enough temperatures, the structure is an array of nearly regular hexagonal domains of roughly the same size. However, as the temperature of the system is lowered, the structure does not reproduce that on the heating curve, even when the system is allowed to anneal for about 25 000 time steps between heating and cooling steps. Between the lowest ($T \approx 0$ K) and highest ($T \approx 100$ K) temperatures, there are about 25–30 annealing steps. Upon cooling, the system remains in the incommensurate phase, although the lowest energy state at $T = 0$ K is clearly the commensurate one. Long runs (up to 2×10^6 time steps) often show continuing relaxation of the system. This relaxation occurs at the transition from the commensurate to the incommensurate solid. At the higher temperatures used for the structure factor [$S(\mathbf{q})$] calculations, the simulations show little evidence of significant hysteresis.

For temperatures near 60 K, the average structure of the unconstrained system is reproducible enough that reliable estimates of $S(\mathbf{q})$ are obtained. The $S(\mathbf{q})$ are calculated from runs of about 10^5 time steps, sampling every 100 steps. Sometimes, to test the effects of relaxation, the sampling begins after 2×10^6 equilibrating steps. The average lattice constant is determined to $\Delta L_u \approx \pm 0.01$ Å and the orientation to $\Delta\vartheta \approx 0.1^\circ$ at $T \approx 60$ K. The L_u is in the range of 4.45–4.47 Å, relatively independent of the value of V_g . These results agree with the QHT values in Table II to 0.02 Å. When nonzero, ϑ is about $0.2^\circ - 0.4^\circ$, relative to the commensurate orientation. This angle tends to fluctuate during the simulation, perhaps indicating that the system jumps back and forth between two or more orientations as the simulation proceeds.

2. Domains and mappings

The configurations of the finite temperature MD simulations can be analyzed in a number of ways for evidence of

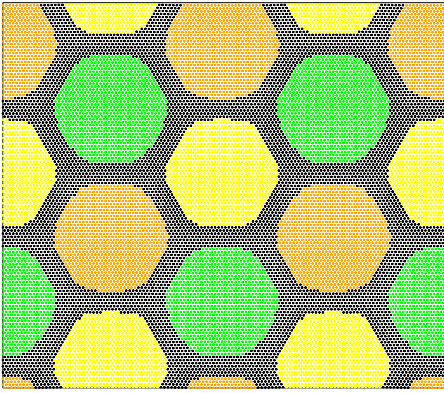


FIG. 2. (Color online) Domains and domain walls for HI structure with moderate linear misfit $m \approx 0.016$ and low temperature ($T < 1$ K), $V_g = -5$ K and pair potential and cell as in Fig. 1. The reduced density is $\theta = 0.9695$, and the average lattice is a regular hexagon with $L = 4.3274$ Å. Plot is for the time-averaged positions.

domain structure. The simplest approach is to look at the domain structure in direct space, examining both the instantaneous positions and the time-averaged positions using a four-color map. Given the periodic boundary conditions, the calculation of the time-averaged positions needs to be done with some care to correct for the movement of particles across the boundary. Results reported here are typically generated by averaging the positions from simulation runs of about 100 000 time steps (3.26 ns). This is generally long enough to average out the thermal motion of the adatoms. The rules used to assign the adatom positions on the map are as follows. A (somewhat arbitrary) reference distance of one-fourth of the graphite lattice constant ℓ is used to determine which sublattice to associate with any given adatom. That is, if the adatom distance from the nearest adsorption site is less than $\ell/4$, the adatom is assigned to the sublattice of that adsorption site. If the adatom is further than $\ell/4$ from any adsorption site, it is assigned to a domain wall. There are three sublattices for the adsorption of the xenon atom, and the assignment of an adatom to a sublattice is displayed in a color unique to that sublattice, while a fourth color is used for adatoms that are assigned to a domain wall. Domains and domain walls clearly stand out, especially for the time-averaged positions. The instantaneous positions show a more irregular structure as a result of thermal motions but, even then, the four-color map displays the basic topology of the structure. With this scheme, a uniform hexagonal lattice that is incommensurate with the substrate generates a map that has domain wall widths about equal to the domain sizes. Systems with a well-developed domain structure have domain walls that are narrower or much narrower than the domain size and, especially at low temperature, the domains themselves have the expected hexagonal shape.

For the MD simulations of the constrained system, the domain topology is dominated by the hexagonal network of (superlight) domain walls that is characteristic of the HI phase. Figure 2 shows a map for moderate misfit and low temperature using the time-averaged positions. It has a very regular HI structure with clearly defined domains and domain walls.³⁷ On the other hand, when the misfit has the

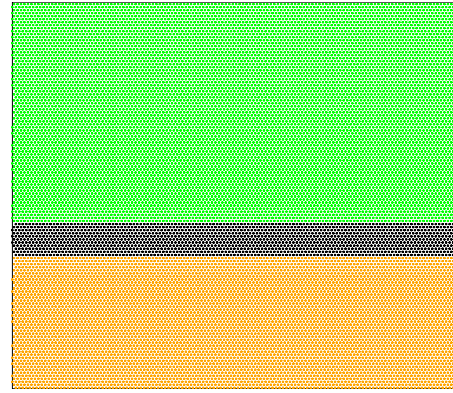


FIG. 3. (Color online) Domains and domain walls for single wall case (very small uniaxial misfit $m = 0.0052$) and low temperature ($T < 1$ K), $V_g = -5$ K and pair potential and cell as in Fig. 1. Plot is for the time-averaged positions.

smallest value consistent with the boundary conditions (with the superlattice constraint, only certain densities are allowed), there typically is a single wall which is roughly parallel to one of the boundary walls and is almost always along the \hat{x} axis. Figure 3 shows such a case. The stability of the uniaxially dilated lattice is sensitive to the boundary conditions and, except for the smallest misfits, the lattice reorganizes into a 2D HI array of misfit when the system size is increased. For instance, when the size of the system is increased by doubling the lengths of the sides (the system is also reinitialized and annealed), the single wall case occurs at a new density which is that of the smallest nonzero misfit allowed by the boundary conditions, but at all other misfits the hexagonal structure is found. Further, the domains of the smallest misfit systems (typically at $m \leq 0.005$ for the 16 K system) are irregular hexagons even at $T = 0$ K. In such cases, e.g., Fig. 4, the linear dimensions of the domains are comparable to the linear size of the system, which suggests that system size and periodic boundary conditions are affecting

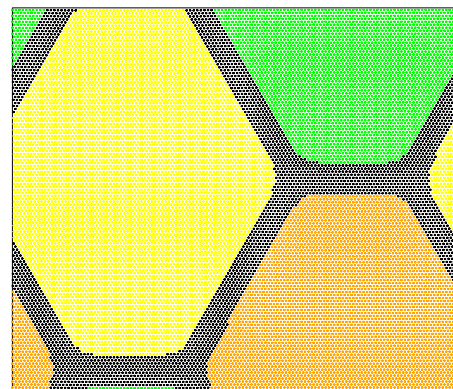


FIG. 4. (Color online) Domains and domain walls for HI structure with small linear misfit and low temperature ($T < 1$ K), $V_g = -5$ K and pair potential and cell as in Fig. 1. The reduced density is $\theta = 0.9870$ and the fractional misfit is $m = 0.0078$ along \hat{x} and $m = 0.0052$ along \hat{y} , so the domain structure is not regular hexagons. Plot is for the time-averaged positions.

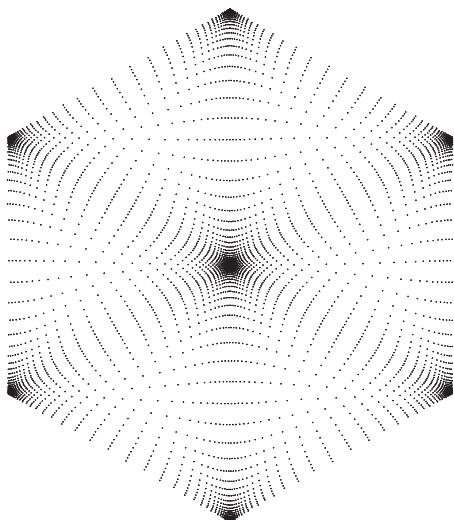


FIG. 5. Return map for the regular HI structure with moderate linear misfit and low temperature ($T < 1$ K) with domains shown in Fig. 2. Plot is for the time-averaged positions.

the geometry of walls. The domain wall structure becomes more regular as the (two-dimensional) misfit increases, and for the largest misfits examined here, the array has nearly regular hexagons. Nonetheless, the effect of system size on the energy per adatom is small for the sizes and misfits used in this work.

A second mapping technique also clearly distinguishes the hexagonal and uniaxial structures. The mapping is defined by starting with the position of each adatom and using the primitive translational vectors of the commensurate lattice to map each position into the Wigner-Seitz cell of the commensurate phase. This cell is a hexagon with its center associated with one sublattice. Three of its vertices (forming an equilateral triangle with one vertex up) are associated with another sublattice, and the other three vertices (forming an equilateral triangle with one vertex down) are associated with the third sublattice. A uniform hexagonal lattice, incommensurate with the substrate, generates a uniform distribution of points in the hexagon. A true HI structure gives a high density of points surrounding the center and vertices of the hexagon (resulting from many atoms near adsorption sites) and broad lines with a high density of points connecting the vertices to each other along the edges and connecting the vertices to the center. This can be seen in Fig. 5. For the time-averaged positions, the map points lie along distinct, wavy lines instead of being smeared out. The pattern becomes less distinct as the temperature of the system is increased, even for the time-averaged positions. In contrast, the map for the UIC structure has stripes parallel to the \hat{y} axis and connecting two or more sublattice points, e.g., Fig. 6. This mapping technique can be used on both the instantaneous and the time-averaged positions; it has much in common with return maps and Poincaré sections and was motivated by those maps. Although such maps might also show the existence of chaotic behavior, no evidence of chaos, other than normal thermal chaos, was found in the Xe/graphite simulations.

A third approach to the determination of the structure is simply to calculate the static structure factor, as described in

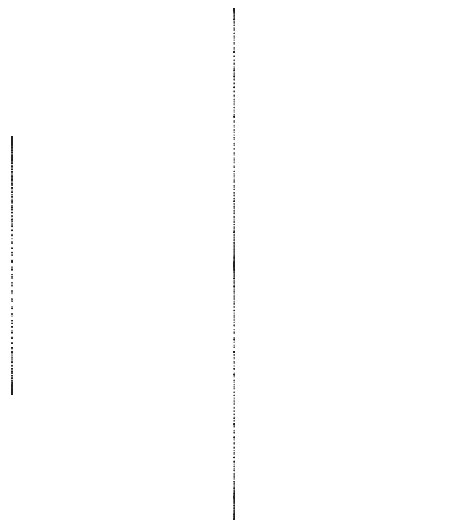


FIG. 6. Return map for UIC structure with small linear misfit and low temperature ($T < 1$ K), $\theta = 0.9935$; $m = 0.0066$, $V_g = -5$ K, and pair potential and cell as in Fig. 1. Plot is for the time-averaged positions.

IV C 1. This is a very time consuming calculation, so it was done only at selected n, T pairs. Our $S(\mathbf{q})$ results generally confirm the results of the other two approaches.

3. Relative stability of uniaxially incommensurate and hexagonal incommensurate

The MD approach finds the equilibrium structure of the system if there are no metastable states. Thus, to compare the energies of the UIC and HI domain wall arrays at similar densities requires some constraint to stabilize both structures. This is done here by a judicious choice of boundary conditions in which the system is forced into the UIC structure by using a very long and thin simulation cell. Because these boundary conditions severely constrain the thermal excitations of the domain walls, only the zero temperature classical energies are reliable. To avoid differences that might arise due to changes in the radius used to limit the force calculation or the radius used to build the nearest-neighbor list, the minimum width in the \hat{x} direction must accommodate about ten columns of xenon atoms. A length along the \hat{y} axis corresponding to 1024 rows of xenon atoms in the periodic cell gives a reasonably fine density grid. With these parameters, a UIC phase is stabilized for a range of relative densities, $\theta = n/n_c$, from about 0.9523 to about 0.9993. (Systems with $\theta > 1.0$ were not generated since they do not seem relevant to the experiments on Xe/graphite, where the commensurate monolayer is succeeded by a bilayer rather than a further compressed incommensurate monolayer.) With this size and the periodic boundary conditions, the domain walls are parallel to the \hat{x} axis and move dynamically parallel to the \hat{y} axis. Joos *et al.*⁸ also found this to be the optimum orientation of the domain walls for the UIC phase.

The ground-state energy is determined for a specified density of the constrained system using the energies evaluated as a function of the temperature along an isochore as described

in Sec. IV C 1. This yields ground-state energies to at least five significant figures (statistical uncertainty only, not systematic). Figure 1 compares the zero temperature energies of the UIC and HI phases as a function of the area per atom (inverse number density) for $V_g = -5.0$ K. The HI phase is definitely the more stable one over most of the density range shown, as the energy differences at moderate to large misfits are much greater than the uncertainties in the energies. At $\theta = 0.9523$, the UIC phase is higher in energy than the HI phase by about 4 K per xenon. Further, as the density approaches that of the commensurate phase, the two curves cannot be distinguished within statistical uncertainty. While we have not made a thorough examination of the entire parameter space, preliminary full nonlinear SCP-MDW calculations are consistent with the assertion that for the range of V_g and misfit values considered here, the HI phase is the stable phase. On the other hand, the general behavior of the simulations leaves the reservation that the relative stability at very small misfit might be altered by changes in the boundaries of the theoretical models, or in the experimental conditions, that caused changes of order of 0.1 K per atom in the relative energies.

V. CONCLUDING REMARKS

With an estimate of $V_g \approx -6$ K, based on the discussion in Sec. IV B, the corrugation energy of Xe/graphite from minimum to maximum is $E_{corr} = 54$ K (48 K from minimum to saddle). A recent electronic energy calculation¹⁵ gives 73 K for the increment from minimum to maximum of Xe/graphite. Estimates³ for some related systems are $E_{corr} \approx 55$ K for krypton/graphite and 200–300 K for Xe/Pt(111).

We have concluded that the HI \rightarrow C transition for Xe/graphite is continuous as the pressure increases. There are two qualitative theoretical discussions that come to the opposite conclusion. The first, by Bak *et al.*,⁶ is based on ideas of attractive wall-wall intersections, and the schematic energy-misfit diagram is contrary to what the calculations of Joos *et al.*⁸ and our Fig. 1 show. While we cannot exclude that their scenario might arise at very small misfit ($m \ll 0.005$), the calculations with realistic interaction models do exclude it for $m > 0.005$ and thus disagree with the experimental findings of Hong *et al.*⁵ and agree with those of Hamichi *et al.*⁴ The second, by Coppersmith *et al.*,³⁶ shows that a weakly incommensurate solid (HI with small misfit) should be unstable with respect to the spontaneous formation of dislocations and thus that there should be a fluid phase between the C and HI solids. We can only remark that the lattices of the QHT series are dynamically stable at misfits down to $m = 0.017$ (although a zero temperature consideration) and that the compressed lattices with small misfit of the MD series show no dynamical anomalies. The unconstrained (isolated patch) simulations for the larger two values of $|V_g|$ show significant hysteresis as the system progresses from a commensurate structure to an incommensurate one, and, in the initial stages of this progression, the wall structures are irregular with no clear structural pattern. Whether this is a signal of the predicted instability is difficult to say.

However, the most extensive analysis of electron diffraction line shapes for Xe/graphite at small misfit and 60 K does not give any evidence for mobile dislocations.³⁸

ACKNOWLEDGMENTS

We would like to thank the Computer Science Department at Lafayette College for the use of their research cluster which is supported, in part, by NSF Grant No. DIB 0442269. One of us (L.W.B.) has had several helpful conversations about this work with J. A. Venables, R. Kariotis, and S. N. Coppersmith.

APPENDIX: ZERO-ORDER SELF-CONSISTENT-PHONON, MASS-DENSITY-WAVE APPROXIMATION

The self-consistent-phonon (SCP) calculation for a monolayer with mass-density-wave (MDW) distortions has been described earlier for the case of small amplitude distortions using a linear response approximation to evaluate the MDW terms, denoted paper I.⁹ The extension of the MDW approach to the nonlinear regime has been described for a one-dimensional classical system in paper II.¹⁰ The SCP-MDW approximation used here is a partial melding of those two approaches and is the lowest-order approximation to an extension of the work in II to two dimensions and also to systems where quantum effects cannot be ignored. We use the notations of papers I and II in describing how the current SCP-MDW calculations are carried out.

Starting with the SCP calculation in paper I,⁹ the first modification occurs with Eq. (I23). That equation is obtained by carrying out a power series expansion of the exponential term in Eq. (I19) that depends on the average displacement of the atoms from the parent lattice positions. As described in paper II, a better starting point for this term is the Bessel function expansion written out in Eq. (II6) and explained in detail in the text there. When extended to two dimensions, the arguments of the Bessel functions become scalar products of a given reciprocal lattice vector (\mathbf{g}) of the substrate and the set of MDW displacement Fourier amplitudes (\mathbf{u}_j). Each of these displacement amplitudes is associated with a particular misfit wave vector (\mathbf{q}_j) in the MDW expansion. As described in paper I, there is one such \mathbf{q}_j for each reciprocal lattice vector \mathbf{g}_j associated with a nonzero amplitude in the Fourier expansion for the substrate field. Following the arguments of paper II with respect to the reordering of these Bessel function expansions, we have kept only the lowest-order terms and then implemented the calculation as outlined in paper I. The algebraic details are tedious but the result is relatively transparent, namely, Eq. (I25) is modified by replacing the U_g term in that equation (V_g here) with the more complex expression

$$V_g \prod_{j=1}^6 J_0(\mathbf{g} \cdot \mathbf{u}_j), \quad (\text{A1})$$

where J_0 is the zero order Bessel function of the first kind. The resulting equation for the \mathbf{u}_j is solved by successive iterations.

The main effect of this alteration is to limit the amplitude of the MDW distortions, which the linear response approximation overestimates, and to cause ϑ to remain zero at small but finite misfit. However, the coupling between these distortions, which is present in the full nonlinear expansion,¹⁰ is not present here. For these reasons, the MDW distortions treated here do not generate the higher-order harmonics found in the full nonlinear expansion and thus these MDWs are simple sine wave distortions, one for each vector \mathbf{g}_j used in the expansion of the substrate potential field. Because this

is a low-order expansion, we have restricted the SCP-MDW calculations to moderate and large misfit cases where the MDW amplitudes are relatively small and where the higher harmonic terms, which give rise to distinct domains and narrow domain walls, are not crucial.

Preliminary calculations using the full nonlinear SCP-MDW theory have been used as checks on the SCP-MDW and QHT approximations as well as the MD results. No serious discrepancies have been observed.

-
- ¹J. Suzanne and J. M. Gay, in *Physical structure of solid surfaces*, edited by W. N. Unertl, Handbook of Surface Science Vol. 1 (North-Holland, Amsterdam, 1996), Chap. 10, pp. 503–75.
- ²L. W. Bruch, M. W. Cole, and E. Zaremba, *Physical Adsorption: Forces and Phenomena* (Oxford University Press, Oxford, 1997).
- ³L. W. Bruch, R. D. Diehl, and J. A. Venables, *Rev. Mod. Phys.* **79**, 1381 (2007).
- ⁴M. Hamichi, A. Q. D. Faisal, J. A. Venables, and R. Kariotis, *Phys. Rev. B* **39**, 415 (1989).
- ⁵We note that there are contradictory experiments that are interpreted to give a first order transition with a lattice constant discontinuity of 1%. However, those are closed cell thermodynamic systems and are not as conceptually simple as the experiments of Hamichi *et al.*, See H. Hong, R. J. Birgeneau, and M. Sutton, *Phys. Rev. B* **33**, 3344 (1986); H. Hong, C. J. Peters, A. Mak, R. J. Birgeneau, P. M. Horn, and H. Suematsu, *ibid.* **36**, 7311 (1987); and Sec. V E 1 of Ref. 3.
- ⁶P. Bak, D. Mukamel, J. Villain, and K. Wentowska, *Phys. Rev. B* **19**, 1610 (1979).
- ⁷J. Villain and M. B. Gordon, *Surf. Sci.* **125**, 1 (1983).
- ⁸B. Joos, B. Bergersen, and M. L. Klein, *Phys. Rev. B* **28**, 7219 (1983).
- ⁹A. D. Novaco, *Phys. Rev. B* **19**, 6493 (1979).
- ¹⁰A. D. Novaco, *Phys. Rev. B* **22**, 1645 (1980).
- ¹¹A. K. Dham, W. J. Meath, A. R. Allnatt, R. A. Aziz, and M. J. Slaman, *Chem. Phys.* **142**, 173 (1990).
- ¹²A. D. McLachlan, *Mol. Phys.* **7**, 381 (1964).
- ¹³K. Pussi, J. Smerdon, N. Ferralis, M. Lindroos, R. McGrath, and R. D. Diehl, *Surf. Sci.* **548**, 157 (2004).
- ¹⁴T. Mandel, M. Domke, G. Kaindl, C. Laubschat, M. Prietsch, U. Middelmann, and K. Horn, *Surf. Sci.* **162**, 453 (1985).
- ¹⁵J. L. F. Da Silva and C. Stampfl, *Phys. Rev. B* **76**, 085301 (2007).
- ¹⁶L. W. Bruch, P. I. Cohen, and M. B. Webb, *Surf. Sci.* **59**, 1 (1976); L. W. Bruch, *ibid.* **125**, 194 (1983).
- ¹⁷The values derived from the model potentials depend sensitively on the value of z that is used. The following results are the values at z that corresponds to the ground state (potential energy plus zero point energy) of $V_0(z)$ for models of W. A. Steele, *Surf. Sci.* **36**, 317 (1973) and M. L. Klein, S. O'Shea, and Y. Ozaki, *J. Phys. Chem.* **88**, 1420 (1984). The values are -3.8 K for the Steele model and -7.5 K for that of Klein *et al.* When the substrate anisotropy is included² with $\gamma_a=0.4$ and $\gamma_R=-0.54$, the values change to -6.2 K (at $z=3.72$ Å) and -12.3 K (at $z=3.39$ Å), respectively.
- ¹⁸H. Hong, C. J. Peters, A. Mak, R. J. Birgeneau, P. M. Horn, and H. Suematsu, *Phys. Rev. B* **40**, 4797 (1989).
- ¹⁹R. D. Boutchko and L. W. Bruch, *Phys. Rev. B* **70**, 195422 (2004).
- ²⁰These are aligned along the $\psi_s=30^\circ$ symmetry azimuth of F. Grey and J. Bohr, *Europhys. Lett.* **18**, 717 (1992).
- ²¹K. L. D'Amico, J. Bohr, D. E. Moncton, and D. Gibbs, *Phys. Rev. B* **41**, 4368 (1990). These authors also report a diffraction pattern at 65 K with $L=4.47$ Å; since the monolayer might be under compression, this may be a lower bound to L_u at 65 K.
- ²²A. A. Maradudin, E. W. Montroll, G. H. Weiss, and I. P. Ipatova, *Theory of Lattice Dynamics in the Harmonic Approximation* (Academic, New York, 1971).
- ²³L. W. Bruch and M. S. Wei, *Surf. Sci.* **100**, 481 (1980). In the calculations, the 45 points are unfolded to 81 points so that no assumption is made about the symmetry of the basis in the hexagonal unit cell.
- ²⁴D. Frenkel and B. Smit, *Understanding Molecular Simulation: From Algorithms to Applications*, Computational Science Series Vol. 1 (Academic, London, 2002).
- ²⁵J. M. Phillips and L. W. Bruch, *J. Chem. Phys.* **83**, 3660 (1985).
- ²⁶Assuming this smoothness amounts to neglect of effects of the Peierls pinning potential.
- ²⁷Equation (7) is a quadratic equation for ξ . We discard the second root because it corresponds to $\xi > 1/3$, a range where the truncation of Eq. (3) at second order is no longer accurate.
- ²⁸T. H. Ellis, G. Scoles, U. Valbusa, H. Jónsson, and J. H. Weare, *Surf. Sci.* **155**, 499 (1985).
- ²⁹C. W. Mowforth, T. Rayment, and R. K. Thomas, *J. Chem. Soc., Faraday Trans. 2* **82**, 1621 (1986).
- ³⁰J. Unguris, L. W. Bruch, E. R. Moog, and M. B. Webb, *Surf. Sci.* **87**, 415 (1979).
- ³¹These values are taken from the chemical potential vs. temperature phase diagram presented as Fig. 19 in Ref. 3 and are based mostly on data of Hamichi *et al.* (Ref. 4) and Suzanne *et al.* (Ref. 33).
- ³²J. Suzanne, J. P. Coulomb, and M. Bienfait, *Surf. Sci.* **47**, 204 (1975).
- ³³J. Suzanne, J. P. Coulomb, and M. Bienfait, *Surf. Sci.* **44**, 141 (1974).
- ³⁴R. Kariotis, J. A. Venables, M. Hamichi, and A. Q. D. Faisal, *J. Phys. C* **20**, 5717 (1987).
- ³⁵The experimental lattice constants of Ellis *et al.* and Mowforth *et al.* probably strengthen this to excluding $V_g \leq -8$ K. The QHT free energy minimum for $V_g = -8$ K at 10 K is an incommensu-

rate solid with $L_u=4.36$ Å. Then, the interpolated value for L_u at 15 K is 1.4% smaller than the lattice constant reported by Ellis *et al.* (Ref. 28), a margin large enough to be a basis for excluding $V_g=-8$ K.

³⁶S. N. Coppersmith, D. S. Fisher, B. I. Halperin, P. A. Lee, and W. F. Brinkman, Phys. Rev. B **25**, 349 (1982).

³⁷B. Grimm, H. Hövel, M. Pollmann, and B. Reihl, Phys. Rev.

Lett. **83**, 991 (1999) show a pattern of hexagonal Xe/ graphite domains at 5 K with walls tilted by 11° and spaced by 5 nm. If the walls are superlight, the structure has $\vartheta=0.54^\circ$ and $L=4.48$ Å. Such a structure corresponds to one detected in electron diffraction by Hamichi *et al.* (Ref. 38) at $T\approx 75$ K.

³⁸M. Hamichi, R. Kariotis, and J. A. Venables, Phys. Rev. B **43**, 3208 (1991).